Journal of Sound and Vibration (2000) **236**(1), 61–87
doi:10.1006/jsvi.2000.2959, available online at http://www.idealibrary.com on IDEAL®

DYNAMIC RESPONSES OF RAILWAY AND CARRIAGE UNDER THE HIGH-SPEED MOVING LOADS

JONG-SHYONG WU AND PO-YUN SHIH

Institute of Naval Architecture and Marine Engineering, National Cheng-Kung University, Tainan, Taiwan 701, *Republic of China*

(*Received* 19 *October* 1999, *and in final form* 24 *January* 2000)

The dynamic responses of the railway and the carriage due to action of the multi-roller carriage were determined by means of the finite element method. Based on the dynamic equilibrium of a carriage and its suspension systems, the property matrices for the carriage were derived. The assembly of the last property matrices and those for the railway together with the elastic foundation yields the "time-dependent" overall property matrices and the equations of motions for the entire vibrating system, where the external loads on the railway are composed of the gravity forces due to axle rollers and carriage. By using the direct integration method, the equations of motions were solved to give the dynamic responses of the railway and the carriage. Since the effects of inertial forces due to the moving loads (carriage together with the axle rollers) and the effects of springs and dampers for the suspension systems are all considered and the total number of the axle rollers ranges from 2 to 4, the formulation of this paper may be the closest one in agreement with the practical situations among the existing literature. Therefore, the presented theory should be significant for the design of railway tracks.

1. INTRODUCTION

A "massless" elastic foundation in which compressive and tensile reactions are admissible is called the Winkler foundation [1]. Based on this hypothesis the dynamic response of the railway tracks has been studied by many researchers. Here only some of the relevant literature was mentioned. Criner and McCann [2] presented an electric-analog-computer technique for the analysis of beams on elastic foundations and subjected to travelling forces. Kenney and Pasadena [3] studied a similar problem with an analytical solution and resonance diagrams, where the effect of viscous damping was also considered. Florence [4] obtained the wave solution by using the Laplace-transform method for a semi-infinite beam. In addition to a harmonic concentrated exciting force, Patil [5] and Duffy [6] studied the effect of mass of the load on the dynamic response of an infinite beam on the Winkler foundation, but Patil's solution is available only for the stationary load. To realize the influence of the foundation mass, Patil [7] determined the natural frequencies of an infinite beam resting on a three-dimensional "inertial" elastic foundation.

Some researchers thought that the Winkler foundation was not realistic and presented a new foundation called "tensionless Winkler foundation". Since such a foundation cannot transmit tensile forces across the interface between the supporting and supported members, separation of track from the foundation will occur under certain conditions. Based on the tensionless Winkler foundation, Weitsman [8, 9] presented several examples to prove that

0022-460X/00/360061 + 27 $35.00/0

the absence of tensile forces may be accompanied by the formation of "no contact regions". For an infinite beam resting on a flat rigid foundation and subjected to an "upward" concentrated moving force, Adams and Bogy [10] computed and illustrated graphically the non-contact lengths, mode shapes and foundation reactions. To replace the "upward" concentrated moving force by the "downward" one, the same problem was studied by Choros and Adams [11].

All the foregoing problems were solved with the analytical methods except that of reference [2]. However, for most of the engineering problems, the analytical methods are usually not available and must rely on the numerical methods. Although the finite element method (FEM) has already been used for the dynamic analysis of structures such as bridge [12], beam [13], plate [14], etc., application of the FEM to the dynamic analysis of the "infinite" railway tracks is rare because the "infinite" degrees of freedom (d.o.f) of the "infinite" railway track prevents the availability of the FEM. For this reason, based on the equivalence between the resonant frequency, the critical moving speed, the frequency spectrum and the maximum forced vibration responses of the finite railway and those of the infinite one, the present authors replaced the infinite railway by a finite one so that the FEM is available for the dynamic analysis of the finite railway [15]. Hence, the dynamic behaviors of the finite railway studied in this paper are very close to those of the infinite one.

The research on the inertial effects of the moving loads is rare. In addition to references [5] and [6], Michaltsos *et al.* [16] studied the inertial effect of a moving mass on the dynamic response of a simply supported beam, Esmailzadeh *et al.* [17] studied a similar problem by replacing the point mass with the uniform partially distributed moving masses. In both references [16, 17], the problem was solved by using the series solution method incorporated with the conventional analytical technique. For a simply supported beam on an elastic foundation and subjected to a moving load, Thambiratnam and Zhuge [18] studied the inertial effect of the moving load with FEM. In reference [19], Krylov investigated the vibration characteristics of the track and the ground for the infinite railway analytically by considering the effect of the sleepers and neglecting that of the inertial force of the single axle load.

In most of the existing literature [1–11, 16, 17, 19], the total number of moving loads is single and the dynamic response of the load itself was neglected. To accommodate the practical applications, the dynamic responses of the railway together with the carriage subjected to the action of a railway carriage with 2–4 suspension systems are studied in this paper. Effects such as the inertial forces due to carriage and axle loads, and the elastic forces and the damping forces due to the springs and dampers of the suspension systems, were all taken into account in the formulation of the problem.

2. PROPERTY MATRICES FOR THE RAILWAY AND ITS FOUNDATION

Figure 1 shows the mathematical model for a finite railway track resting on the Winkler foundation with linear spring constant k_w, where $\overline{oxyz}$ is the global co-ordinate system, L is the total length of the railway, ℓ is the length of each beam element and the solid circles (●) denote the nodes for the beam elements. The nth element was enlarged and shown in Fig. 2, where $\bar{x}_1^{(n)}$ and $\bar{x}_2^{(n)}$ denote the distances from the left end of the railway (point $\bar{o}$) to node ① and node ② of the nth beam element respectively. For convenience, a local co-ordinate system ①xyz was introduced. The distance from the left end of the beam element (node ①) to any cross-section of the beam element is represented by x, and the distance from node ① to the ith linear spring is denoted by x_i respectively.

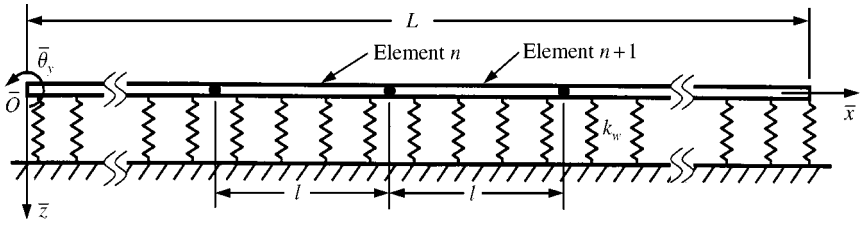

Figure 1. The mathematical model for a finite railway.

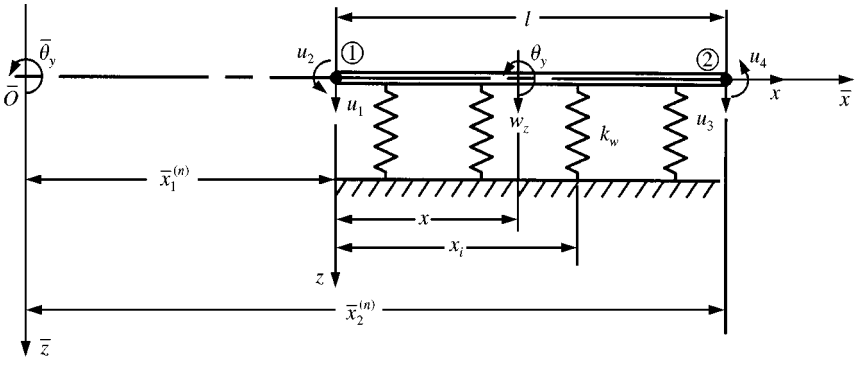

Figure 2. Definitions for the element displacements, w_z and θ_y, the node displacements u_j ($j = 1$–4) and the relevant notations.

2.1. ELEMENT STIFFNESS MATRIX

For the present problem, the potential energy of the beam element together with the supporting linear springs is given by

$$U = \frac{1}{2}\int_0^{\ell} EI_y\theta_{y,x}^2\,\mathrm{d}x + \frac{1}{2}\sum_{i=1}^{n_e} k_w w_z^2(\xi_i, t), \tag{1}$$

where E is Young's modulus of the railway material, I_y is the moment of inertia of the cross-sectional area of the railway (about the y-axis), w_z is the vertical deflection of the beam element (in the z direction), θ_y is the slope of the beam element (about the y-axis), $\theta_{y,x} = \partial\theta_y/\partial x$, k_w is the spring constant of each linear spring, $\xi_i = x_i/\ell$ and n_e is the total number of linear springs supporting the beam element.

From reference [20], one has

$$w_z(\xi, t) = \{a_z(\xi)\}^{\mathrm{T}}\{u(t)\}, \tag{2a}$$

$$\theta_y(\xi, t) = \{a_y(\xi)\}^{\mathrm{T}}\{u(t)\}, \tag{2b}$$

where

$$\{a_z(\xi)\} = \{a_{z1}(\xi) \quad a_{z2}(\xi) \quad a_{z3}(\xi) \quad a_{z4}(\xi)\}, \tag{3a}$$

$$\{a_y(\xi)\} = \{a_{y1}(\xi) \quad a_{y2}(\xi) \quad a_{y3}(\xi) \quad a_{y4}(\xi)\}, \tag{3b}$$

$$\{u(t)\} = \{u_1(t) \quad u_2(t) \quad u_3(t) \quad u_4(t)\}. \tag{3c}$$

In the last expressions, $u_i(t)$ $(i = 1–4)$ are the nodal displacements shown in Figure 2 and a_{zi} and a_{yi} are the associated shape functions [20].

The substitution of equations (2a) and (2b) into equation (1) results in

$$U = \tfrac{1}{2}\{u\}^{\mathrm{T}}[k]\{u\}, \tag{4}$$

where

$$[k] = [k]_1 + [k]_2, \tag{5}$$

$$[k]_1 = \int_0^{\ell} EI_y\{a_{y,x}\}\{a_{y,x}\}^{\mathrm{T}}\,\mathrm{d}x, \tag{6}$$

$$[k]_2 = \sum_{i=1}^{n_e} k_w\{a_z(\xi_i)\}\{a_z(\xi_i)\}^{\mathrm{T}}. \tag{7}$$

In the last equations, $[k]_1$ is the stiffness matrix of the beam element alone, $[k]_2$ is the stiffness matrix due to the n_e linear springs supporting the beam element, and the combination of $[k]_1$ and $[k]_2$ defines the effective stiffness matrix of a beam element for the railway supported by the linear springs as shown in Figure 1. The notations $\{\,\}$ and $[\,]$ appearing in the last equations denote the column vector and the rectangular matrix respectively.

2.2. ELEMENT MASS MATRIX

If the consistent mass model is employed, the element mass matrix of the beam element shown in Figure 2 is given by [20]

$$[m] = \int \rho[a]^{\mathrm{T}}[a]\,\mathrm{d}V = \frac{\rho\bar{A}\ell}{420}\begin{bmatrix} 156 & -22\ell & 54 & 13\ell \\ -22\ell & 4\ell^2 & -13\ell & -3\ell^2 \\ 54 & -13\ell & 156 & 22\ell \\ 13\ell & -3\ell^2 & 22\ell & 4\ell^2 \end{bmatrix}, \tag{8a}$$

where ρ is the mass density of the railway, $\bar{A}$ is the cross-sectional area of the railway and

$$[a] = \begin{bmatrix} \{a_z(\xi)\} \\ \{a_y(\xi)\} \end{bmatrix}. \tag{8b}$$

3. PROPERTY MATRICES FOR A RAILWAY CARRIAGE

For a multi-roller carriage resting on the railway, the mathematical model is shown in Figure 3, where G is the center of gravity (c.g.) of the carriage, m_{ev} and J_{ev} denote the effective mass and mass moment of inertia of the vth carriage, F_v and M_v are the external force and moment, u_v and θ_v are the vertical displacement and rotation angle of the vth carriage at the c.g. of carriage, G respectively. The carriage is supported by $\bar{n}$ suspension systems and $\bar{n}$ rollers. The damping coefficient and spring constant of the ith suspension system are denoted by c_i and k_i respectively, while the mass of the ith roller is denoted by m_i and the horizontal distance between the ith roller (or ith suspension system) and G is denoted by r_i as shown in Figure 3.

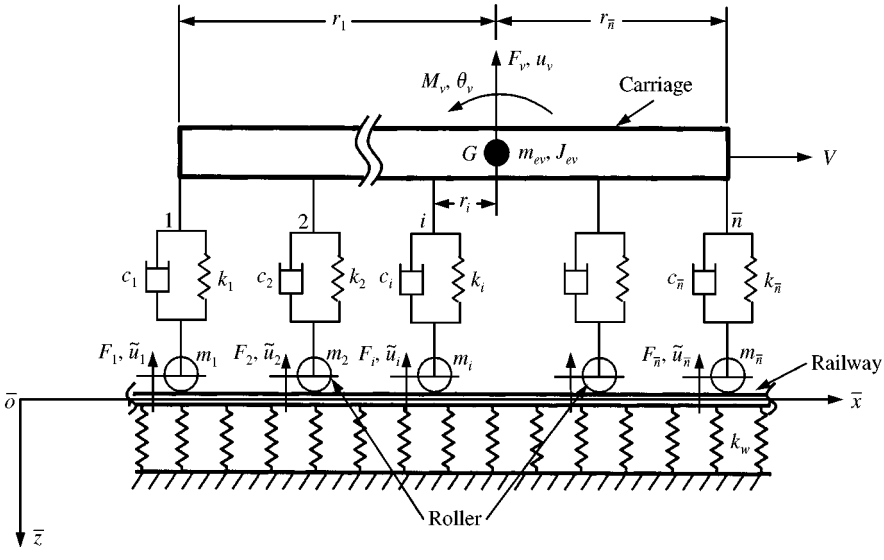

Figure 3. The mathematical model for a moving multi-roller carriage on the railway.

3.1. PROPERTY MATRICES

If the un-sprung masses of roller are assumed to be always in contact with the railway, then the force on the axle of the ith roller is

$$F_i = k_i(\tilde{u}_i - u_v + r_i\theta_v) + c_i(\dot{\tilde{u}}_i - \dot{u}_v + r_i\dot{\theta}_v), \tag{9}$$

where r_i is positive if the ith spring/damper system is located on the left side of G and is negative on the right side of G as shown in Figure 3.

Dynamic equilibrium for the ith roller (m_i) requires that

$$\sum F_{\bar{z}} = F_i + m_i\ddot{\tilde{u}}_i = 0, \tag{10a}$$

while the requirement for the dynamic equilibrium of the rigid carriage (m_{ev} and J_{ev}) is

$$\sum F_{\bar{z}} = \sum_{i=1}^{\bar{n}} F_i + F_v - m_{ev}\ddot{u}_v = 0, \tag{10b}$$

$$\sum M_G = \sum_{i=1}^{\bar{n}} - F_i r_i + M_v - J_{ev}\ddot{\theta}_v = 0. \tag{10c}$$

Substituting equation (9) into equations (10a), (10b) and (10c), one obtains

$$k_i(\tilde{u}_i - u_v + r_i\theta_v) + c_i(\dot{\tilde{u}}_i - \dot{u}_v + r_i\dot{\theta}_v) + m_i\ddot{\tilde{u}}_i = 0, \tag{11a}$$

$$F_v = m_{ev}\ddot{u}_v - \sum_{i=1}^{\bar{n}} F_i = -\sum_{i=1}^{\bar{n}} k_i(\tilde{u}_i - u_v + r_i\theta_v) - \sum_{i=1}^{\bar{n}} c_i(\dot{\tilde{u}}_i - \dot{u}_v + r_i\dot{\theta}_v) + m_{ev}\ddot{u}_v \tag{11b}$$

$$M_v = J_{ev}\ddot{\theta}_v + \sum_{i=1}^{\bar{n}} F_i r_i = \sum_{i=1}^{\bar{n}} k_i r_i(\tilde{u}_i - u_v + r_i\theta_v) + \sum_{i=1}^{\bar{n}} c_i r_i(\dot{\tilde{u}}_i - \dot{u}_v + r_i\dot{\theta}_v) + J_{ev}\ddot{\theta}_v. \tag{11c}$$

Writing equations (11a)–(11c) in the matrix form gives

$$\{F_c\} = [k_c]\{\tilde{u}\} + [c_c]\{\dot{\tilde{u}}\} + [m_c]\{\ddot{\tilde{u}}\}, \tag{12}$$

where

$$\{F_c\} = \{0 \;\; F_v \;\; M_v\}, \tag{13a}$$

$$\{\tilde{u}\} = \{\tilde{u}_i \;\; u_v \;\; \theta_v\}, \tag{13b}$$

$$\{\dot{\tilde{u}}\} = \{\dot{\tilde{u}}_i \;\; \dot{u}_v \;\; \dot{\theta}_v\}, \tag{13c}$$

$$\{\ddot{\tilde{u}}\} = \{\ddot{\tilde{u}}_i \;\; \ddot{u}_v \;\; \ddot{\theta}_v\}. \tag{13d}$$

From equations (12) and (13) one obtains the element stiffness, damping and mass matrices for a multi-roller carriage (see Figure 3) to be

$$[k_c] = \begin{bmatrix} k_i & -k_i & -k_i r_i \\ -k_i & \sum_{i=1}^{\bar{n}} k_i & -\sum_{i=1}^{\bar{n}} k_i r_i \\ -k_i r & -\sum_{i=1}^{\bar{n}} k_i r_i & \sum_{i=1}^{\bar{n}} k_i r_i^2 \end{bmatrix}, \tag{14a}$$

$$[c_c] = \begin{bmatrix} c_i & -c_i & -c_i r_i \\ -c_i & \sum_{i=1}^{\bar{n}} c_i & -\sum_{i=1}^{\bar{n}} c_i r_i \\ -c_i r & -\sum_{i=1}^{\bar{n}} c_i r_i & \sum_{i=1}^{\bar{n}} c_i r_i^2 \end{bmatrix}, \tag{14b}$$

$$[m_c] = \begin{bmatrix} m_i & 0 & 0 \\ 0 & m_{ev} & 0 \\ 0 & 0 & J_{ev} \end{bmatrix}. \tag{14c}$$

For the case of $\bar{n} = 4$, $r_1 = a_1$, $r_2 = a_2$, $r_3 = -a_3$ and $r_4 = -a_4$, as shown in Figure 3, one has

$$\{F_c\} = \{0 \;\; 0 \;\; 0 \;\; 0 \;\; F_v \;\; M_v\}, \tag{15a}$$

$$\{\tilde{u}\} = \{\tilde{u}_1 \;\; \tilde{u}_2 \;\; \tilde{u}_3 \;\; \tilde{u}_4 \;\; u_v \;\; \theta_v\}, \tag{15b}$$

$$\{\dot{\tilde{u}}\} = \{\dot{\tilde{u}}_1 \;\; \dot{\tilde{u}}_2 \;\; \dot{\tilde{u}}_3 \;\; \dot{\tilde{u}}_4 \;\; \dot{u}_v \;\; \dot{\theta}_v\}, \tag{15c}$$

$$\{\ddot{\tilde{u}}\} = \{\ddot{\tilde{u}}_1 \;\; \ddot{\tilde{u}}_2 \;\; \ddot{\tilde{u}}_3 \;\; \ddot{\tilde{u}}_4 \;\; \ddot{u}_v \;\; \ddot{\theta}_v\}, \tag{15d}$$

$$[k_c] = k[\alpha], \tag{16a}$$

$$[c_c] = c[\alpha], \tag{16b}$$

$$[m_c] = \lceil m_1 \;\; m_2 \;\; m_3 \;\; m_4 \;\; m_{ev} \;\; J_{ev} \rfloor, \tag{16c}$$

where $\lceil\ \rfloor$ is a diagonal matrix and

$$[\alpha] = \left[\begin{array}{cccc|cc} 1 & 0 & 0 & 0 & -1 & a_1 \\ 0 & 1 & 0 & 0 & -1 & a_2 \\ 0 & 0 & 1 & 0 & -1 & -a_3 \\ 0 & 0 & 0 & 1 & -1 & -a_4 \\ \hline -1 & -1 & -1 & -1 & 4 & -(a_1+a_2-a_3-a_4) \\ a_1 & a_2 & -a_3 & -a_4 & -(a_1+a_2-a_3-a_4) & (a_1^2+a_2^2+a_3^2+a_4^2) \end{array}\right]. \tag{17}$$

3.2. EXTERNAL LOADS ON THE RAILWAY

If the reactive forces on the axles of the rollers m_i ($i = 1$–$\bar{n}$) are represented by F_i', while the static deflection and rotational angle of the carriage are represented by δ_{st} and θ_{st} respectively, as shown in Figure 4, then static equilibrium of the carriage requires that

$$\delta_{st} = \frac{m_{ev}g}{\sum_{i=1}^{\bar{n}} k_i}, \tag{18}$$

$$\sum M_G = \sum_{i=1}^{\bar{n}} - F_i' r_i = 0. \tag{19}$$

Since

$$F_i' = k_i(\delta_{st} + r_i\theta_{st}) \tag{20}$$

the substitution of equation (20) into equation (19) gives

$$\theta_{st} = -\frac{\sum_{i=1}^{\bar{n}} k_i r_i}{\sum_{i=1}^{\bar{n}} k_i r_i^2}\,\delta_{st}. \tag{21}$$

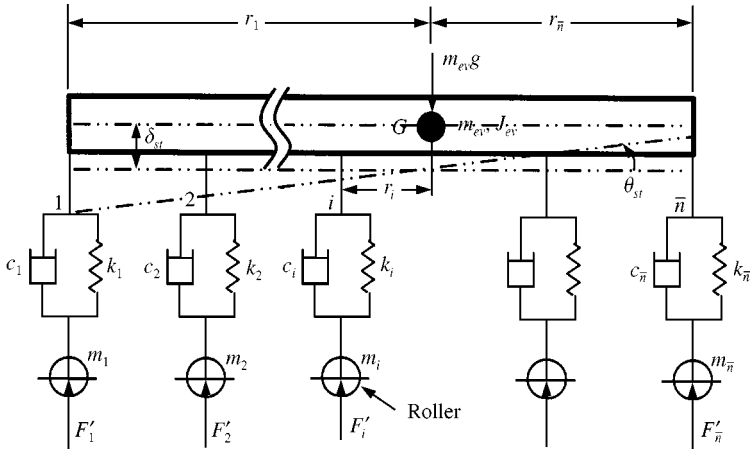

Figure 4. The static deflection and rotational angle of the carriage, δ_{st} and θ_{st}, and the reactive forces on the axles of the rollers, F_i' ($i = 1$–$\bar{n}$).

From equations (18), (20) and (21) one obtains

$$F_i' = k_i\left[1 - \left(\frac{\sum_{i=1}^{\bar{n}} k_i r_i}{\sum_{i=1}^{\bar{n}} k_i r_i^2}\right) r_i\right]\left(\frac{m_{ev} g}{\sum_{i=1}^{\bar{n}} k_i}\right) \tag{22}$$

and the total load on the railway at $r = r_i$ is

$$\bar{F}_{\bar{z}i} = F_i' + m_i g = k_i\left[1 - \left(\frac{\sum_{i=1}^{\bar{n}} k_i r_i}{\sum_{i=1}^{\bar{n}} k_i r_i^2}\right) r_i\right]\left(\frac{m_{ev} g}{\sum_{i=1}^{\bar{n}} k_i}\right) + m_i g \quad (i = 1, 2, \ldots, \bar{n}). \tag{23}$$

For the special case of $k_i = k$ ($i = 1$–$\bar{n}$), equation (23) reduces to

$$\bar{F}_{\bar{z}i} = \left[1 - \left(\frac{\sum_{i=1}^{\bar{n}} r_i}{\sum_{i=1}^{\bar{n}} r_i^2}\right) r_i\right]\left(\frac{m_{ev} g}{\bar{n}}\right) + m_i g \quad (i = 1, 2, \ldots, \bar{n}). \tag{24}$$

4. EQUATIONS OF MOTIONS FOR THE RELEVANT SYSTEMS

4.1. EQUATION OF MOTION FOR THE RAILWAY

Since the element property matrices for the railway together with the foundation have been determined by equations (5)–(8), the assembly of these element property matrices will give the following equation of motion for the whole railway

$$[M]_{N\times N}\{\ddot{\bar{u}}\}_{N\times 1} + [K]_{N\times N}\{\bar{u}\}_{N\times 1} = \{F\}_{N\times 1}, \tag{25}$$

where

$$[K]_{N\times N} = \begin{bmatrix} K_{11} & \cdots & K_{1N} \\ \vdots & \ddots & \vdots \\ K_{N1} & \cdots & K_{NN} \end{bmatrix}_{N\times N}, \tag{26a}$$

$$[M]_{N\times N} = \begin{bmatrix} M_{11} & \cdots & M_{1N} \\ \vdots & \ddots & \vdots \\ M_{N1} & \cdots & M_{NN} \end{bmatrix}_{N\times N}, \tag{26b}$$

$$\{\bar{u}\} = \{\bar{u}_1 \;\; \bar{u}_2 \;\; \cdots \;\; \bar{u}_N\}_{N\times 1} = \{w_1 \;\; \theta_1 \;\; w_2 \;\; \theta_2 \;\; \cdots \;\; w_{\bar{N}} \;\; \theta_{\bar{N}}\}_{N\times 1}, \tag{27a}$$

$$\{\ddot{\bar{u}}\} = \{\ddot{\bar{u}}_1 \;\; \ddot{\bar{u}}_2 \;\; \cdots \;\; \ddot{\bar{u}}_N\}_{N\times 1} = \{\ddot{w}_1 \;\; \ddot{\theta}_1 \;\; \ddot{w}_2 \;\; \ddot{\theta}_2 \;\; \cdots \;\; \ddot{w}_{\bar{N}} \;\; \ddot{\theta}_{\bar{N}}\}_{N\times 1}. \tag{27b}$$

In equations (25)–(27), the notations $\bar{N}$ and N denote the total number of nodes and that of d.o.f. for the whole railway. Since there are two d.o.f. for each node, it is evident that $N = 2\bar{N}$.

For convenience of formulation, the dimension of equation (25) is extended from N to $N' = N + 2$, i.e.,

$$[\bar{M}]_{N'\times N'}\{\ddot{\bar{u}}\}_{N'\times 1} + [\bar{K}]_{N'\times N'}\{\bar{u}\}_{N'\times 1} = \{\bar{F}\}_{N'\times 1}, \tag{28}$$

where

$$[\bar{M}]_{N'\times N'} = \left[\begin{array}{ccc|cc} M_{11} & \cdots & M_{1N} & 0 & 0 \\ \vdots & \ddots & \vdots & \vdots & \vdots \\ M_{N1} & \cdots & M_{NN} & \vdots & \vdots \\ \hline 0 & \cdots & \cdots & 0 & 0 \\ 0 & \cdots & \cdots & 0 & 0 \end{array}\right], \tag{29a}$$

$$[\bar{K}]_{N'\times N'} = \left[\begin{array}{ccc|cc} K_{11} & \cdots & K_{1N} & 0 & 0 \\ \vdots & \ddots & \vdots & \vdots & \vdots \\ K_{N1} & \cdots & K_{NN} & \vdots & \vdots \\ \hline 0 & \cdots & \cdots & 0 & 0 \\ 0 & \cdots & \cdots & 0 & 0 \end{array}\right], \tag{29b}$$

$$\begin{aligned} \{\bar{u}\}_{N'\times 1} &= \{\bar{u}_1 \;\; \bar{u}_2 \;\; \cdots \;\; \cdots \;\; \bar{u}_{N-1} \;\; \bar{u}_N \;\; u_v \;\; \theta_v\}_{N'\times 1} \\ &= \{w_1 \;\; \theta_1 \;\; w_2 \;\; \theta_2 \;\; \cdots \;\; w_{\bar{N}} \;\; \theta_{\bar{N}} \;\; u_v \;\; \theta_v\}_{N'\times 1}, \end{aligned} \tag{30a}$$

$$\begin{aligned} \{\ddot{\bar{u}}\}_{N'\times 1} &= \{\ddot{\bar{u}}_1 \;\; \ddot{\bar{u}}_2 \;\; \cdots \;\; \cdots \;\; \ddot{\bar{u}}_{N-1} \;\; \ddot{\bar{u}}_N \;\; \ddot{u}_v \;\; \ddot{\theta}_v\}_{N'\times 1} \\ &= \{\ddot{w}_1 \;\; \ddot{\theta}_1 \;\; \ddot{w}_2 \;\; \ddot{\theta}_2 \;\; \cdots \;\; \ddot{w}_{\bar{N}} \;\; \ddot{\theta}_{\bar{N}} \;\; \ddot{u}_v \;\; \ddot{\theta}_v\}_{N'\times 1}, \end{aligned} \tag{30b}$$

$$\{\bar{F}\}_{N'\times 1} = \{0 \;\; 0 \;\; \cdots \;\; \cdots \;\; 0 \;\; 0 \;\; 0 \;\; 0\}_{N'\times 1}. \tag{30c}$$

Since all the external loads move with the carriage, they are considered as the coefficients of the external force vector for the carriage, $\{\bar{F}_c\}_{N'\times 1}$ [see equation (37)], rather than those for the railway, for convenience. This is the reason why all the coefficients of $\{\bar{F}\}_{N'\times 1}$ as shown in equation (30c) are equal to zero.

4.2. EQUATION OF MOTION FOR THE CARRIAGE

If the carriage moves on the railway with speed V from left of the railway to right, then the position of the c.g. of the carriage, G, at any time t is given by

$$\bar{x}_G(t) = \bar{x}_0 + r_1 + Vt, \tag{31}$$

where $\bar{x}_0$ is the initial position of the first roller at $t = 0$ and r_1 is the distance between the first roller and G (see Figure 5).

Since the rollers are assumed to contact with the railway always, the vertical displacement of the ith roller, $\tilde{u}_i$, will be equal to that of the node q of the railway, $\bar{u}_{2q-1} = w_q$, if the ith roller applies at node q at time t, i.e.,

$$\tilde{u}_i = \bar{u}_{2q-1} = w_q. \tag{32}$$

It is noted that the subscript $(2q-1)$ indicates the $(2q-1)$th d.o.f. for $\tilde{u}_i$. Since the length of each railway element is ℓ, the d.o.f. of the ith roller is given by

$$N_i = \left(\frac{\bar{x}_G(t) - r_i}{\ell}\right) \times 2 + 1, \quad i = 1, 2, \ldots, \bar{n}, \tag{33}$$

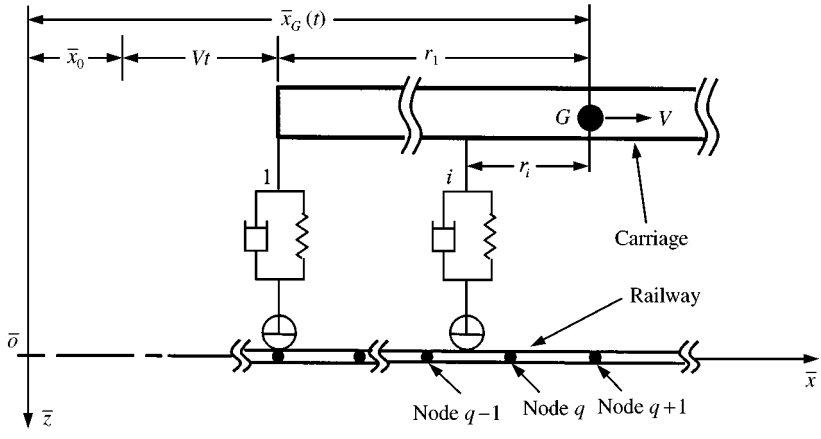

Figure 5. Definitions for the distance $\bar{x}_G(t)$ and the relevant notations.

where r_i is the distance between the ith roller and G, while $\bar{n}$ is the total number of rollers for one carriage. For the case of $\bar{x}_0 = 0$ at $t = 0$, from equations (31) and (33) one obtains $N_1 = 1$ as it should be.

For convenience, we set

$$N_{\bar{n}+1} = N + 1, \quad N_{\bar{n}+2} = N + 2 = N' \tag{34a, b}$$

and extend the dimension of the equation of motion for the carriage (cf. equations (14)–(16)) from $\bar{n} + 2$ to N', i.e.,

$$[\bar{m}_c(t)]_{N'\times N'}\{\ddot{\bar{u}}(t)\}_{N'\times 1} + [\bar{c}_c(t)]_{N'\times N'}\{\dot{\bar{u}}(t)\}_{N'\times 1} + [\bar{k}_c(t)]_{N'\times N'}\{\bar{u}(t)\}_{N'\times 1} = \{\bar{F}_c(t)\}_{N'\times 1}. \tag{35}$$

All the coefficients for the property matrices of equation (35) are equal to zero except the following ones:

$$\bar{X}_{N_i,N_j} = X_{i,j} \quad (i, j = 1, 2, \ldots, \bar{n}, \bar{n} + 1, \bar{n} + 2), \tag{36}$$

where $\bar{X} = \bar{m}_c,\ \bar{c}_c$ or $\bar{k}_c$; $X = m_c,\ c_c$ or k_c; and the values of N_i and N_j are determined by equations (33) and (34), while X_{ij} appearing in equation (36) refer to the coefficients of the property matrices as shown in equation (14) or equation (16).

Likewise, all the coefficients of the external force vector $\{\bar{F}_c(t)\}_{N'\times 1}$ are also equal to zero except the ones below

$$\bar{F}_{cN_i} = \bar{F}_{\bar{z}i} \quad (i = 1, 2, \ldots, \bar{n}), \tag{37a}$$

$$\bar{F}_{cN_{\bar{n}+1}} = F_v, \quad \bar{F}_{cN_{\bar{n}+2}} = M_v, \tag{37b, c}$$

where $\bar{F}_{\bar{z}i}$ $(i = 1\text{–}\bar{n})$ are the external loads on the railway through the rollers of the carriage (see equations (23) and (24)).

In general, the nodal forces $\{\bar{F}_c^{(i)}\}$ induced by a concentrated force $\bar{F}_{\bar{z}i}$ on a beam element are given by [21]

$$\{\bar{F}_c^{(i)}\} = \{a_z(\xi)\}^{\mathrm{T}}\bar{F}_{\bar{z}i}, \tag{38}$$

in which $\{a_z(\xi)\}$ is the shape function given by equation (3a) and $\{\bar{F}_c^{(i)}\}$ is to take the form

$$\{\bar{F}^{(i)}\} = \{f_1^{(i)} \ m_1^{(i)} \ f_2^{(i)} \ m_2^{(i)}\}, \tag{39}$$

where the subscripts 1 and 2 for $f^{(i)}$ and $m^{(i)}$ refer to the nodal force and the nodal moment at nodes ① and ② of the beam element on which $\bar{F}_{\bar{z}i}$ is located, respectively (see Figure 2).

It is evident that one has

$$\{\bar{F}^{(i)}\} = \{\bar{F}_{\bar{z}i} \ 0 \ 0 \ 0\} \tag{40a}$$

if $\bar{F}_{\bar{z}i}$ is located at node ①. Similarly, if $\bar{F}_{\bar{z}i}$ is located at node ②, one has

$$\{\bar{F}^{(i)}\} = \{0 \ 0 \ \bar{F}_{\bar{z}i} \ 0\}. \tag{40b}$$

For simplicity, the locations for the rollers $(r_1, r_2, \ldots, r_{\bar{n}})$, the length of each beam element (ℓ), the moving speed of the carriage (V) and the time interval (Δt) are so selected that all the rollers of the carriage are located at the nodes of the associated beam elements in each computing step. Hence, the external force vector $\{\bar{F}_c\}_{N'\times 1}$ is composed of the element external force vectors to take the form given by equation (40a) or (40b).

4.3. EQUATION OF MOTION FOR THE ENTIRE SYSTEM

The equation of motion for the railway and elastic foundation is determined by equations (28)–(30) and that for the carriage is defined by equations (35)–(37), the combination of these two expressions will lead to the equation of motion for the entire vibrating system

$$[\tilde{M}(t)]_{N'\times N'}\{\ddot{\bar{u}}(t)\}_{N'\times 1} + [\tilde{C}(t)]_{N'\times N'}\{\dot{\bar{u}}(t)\}_{N'\times 1} + [\tilde{K}(t)]_{N'\times N'}\{\bar{u}(t)\}_{N'\times 1} = \{\tilde{F}(t)\}_{N'\times 1}, \tag{41}$$

where

$$[\tilde{M}(t)]_{N'\times N'} = [\bar{M}]_{N'\times N'} + [\bar{m}_c(t)]_{N'\times N'}, \tag{42a}$$

$$[\tilde{C}(t)]_{N'\times N'} = [\bar{c}_c(t)]_{N'\times N'}, \tag{42b}$$

$$[\tilde{K}(t)]_{N'\times N'} = [\bar{K}]_{N'\times N'} + [\bar{k}_c(t)]_{N'\times N'}, \tag{42c}$$

$$[\tilde{F}(t)]_{N'\times 1} = [\bar{F}]_{N'\times 1} + [\bar{F}_c(t)]_{N'\times 1}. \tag{42d}$$

From equation (33) one sees that N_i $(i = 1\text{–}\bar{n})$ is a function of time t, hence all the property matrices and the external force vector of equation (35) are also functions of time as one may see from equations (36) and (37), and so are those of equation (41) for the entire system. For this reason, the present problem is rather complicated and consumes much more computer time than the general problem (with all property matrices being constant) studied in the existing literature [1–16].

5. NUMERICAL RESULTS AND DISCUSSIONS

The mathematical model for this study is shown in Figure 3 and the attention is focused on central vertical displacements of the railway, $w_z(\bar{\xi}, t) = w_z(0{\cdot}5, t)$, and the vertical displacements at the c.g. (G) of the carriage, $w_G(t)$, where $\bar{\xi} = \bar{x}/L$.

The given data for the railway are: Young's modulus $E = 20{\cdot}6 \times 10^{10}$ N/m^2, moment of inertia for the cross-sectional area $I_y = 2{\cdot}037 \times 10^{-5}$ m^4, mass density $\rho = 7850$ kg/m^3, cross-sectional area $\bar{A} = 6{\cdot}37 \times 10^{-3}$ m^2, mass per unit length $\bar{m} = \rho\bar{A} = 50$ kg/m, radius of gyration $\gamma_g = \sqrt{I_y/\bar{A}} = 0{\cdot}032$ m, spring constant for the Winkler foundation $k_w = 3{\cdot}73 \times 10^7$ N/m^2, and length of each beam element $\ell = 1{\cdot}0$ m. While the given data associated with the carriage are: total mass of the carriage $m_{ev} = 2{\cdot}0 \times 10^4$ kg, mass moment of inertia $J_{ev} = 1{\cdot}0 \times 10^4$ kg m^2, mass of each axle roller (or wheel) $m_i = 100{\cdot}0$ kg ($i = 1, 2, \ldots, \bar{n}$), spring constant for each suspension system $k_i = 3{\cdot}0 \times 10^4$ N/m, and damping coefficient for each damper $c_i = 2{\cdot}0 \times 10^4$ N s/m. For convenience, the external loads on the c.g. of carriage (G) are assumed to be zero, i.e., $F_v(t) = M_v(t) = 0$.

5.1. COMPARISON WITH SOME ANALYTICAL SOLUTIONS

For a finite uniform beam (with length L) resting on the elastic foundation and simply supported, the natural frequencies ω_j and the vertical (transverse) displacements $w_z(\bar{\xi}, t)$ at position $\bar{\xi} = \bar{x}/L$ due to a stationary pulsating concentrated force $P(t) = \bar{P}\sin\omega_e t$ applying at $\bar{\xi}_1 = \bar{x}_1/L$ are respectively given by [22]

$$\omega_j = \bar{a}\left(\frac{\pi}{L}\right)^2\sqrt{j^4 + \beta^4}, \quad j = 1, 2, \ldots, \tag{43}$$

$$w_z(\bar{\xi}, t) = \frac{2\bar{P}L^3}{\bar{m}}\sum_{j=1}^{\infty}\sin(j\pi\bar{\xi})\sin(j\pi\bar{\xi}_1)\left[\frac{\sin\omega_e t}{\pi^4\bar{a}^2(j^4 + \beta^4) - \omega_e^2 L^4} - \frac{\omega_e \sin\omega_j t}{L^4\omega_j(\omega_j^2 - \omega_e^2)}\right] \tag{44}$$

where

$$\bar{a}^2 = \frac{EI_y}{\bar{m}}, \quad \beta^4 = \left(\frac{L}{\pi}\right)^4\frac{k_w}{EI_y}. \tag{45a, b}$$

For the railway and elastic foundation studied in this paper with length $L = 100$ m, the lowest 12 natural frequencies ω_j ($j = 1$–12) obtained from equation (43) are shown in column 2 of Table 1, while those obtained from the FEM introduced in this paper are listed in column 3 for the lumped-mass model and in column 4 for the consistent-mass model, respectively. From Table 1 one finds that, among the two FEM models, the natural frequencies obtained from the lumped-mass model are more close to those obtained from equation (43). This is because the assumptions made by the lumped-mass model are more close to those made by equation (43). However, the differences between the values of ω_j ($j = 1$–12) obtained from the lumped-mass model and the corresponding ones obtained from the consistent-mass model are negligible.

If the last railway is subjected to a stationary pulsating force $P(t) = 98000\sin 3t$ N applied at the central point of the railway (i.e. $\bar{\xi}_1 = \bar{x}_1/L = 0{\cdot}5$), the time histories for vertical central displacement $w_z(0{\cdot}5, t)$ of the railway are shown in Figure 6, where the solid, the dashed and the dotted lines denote the time histories obtained from equation (44) (with $j = 1$–1000), the FEM based on the lumped-mass model and the FEM based on the consistent-mass model (with element length $\ell = 1{\cdot}0$ m, time interval $\Delta t = 0{\cdot}01$ s) respectively. It is evident that the dynamic responses of the railway obtained from the FEM (either based on the lumped-mass model or the consistent-mass model) are very close to those obtained from the analytical solution given by equation (44).

TABLE 1

The lowest 12 *natural frequencies of a simply supported beam on elastic foundation*[†]

Mode numbers (j)	Natural frequencies ω_j (rad/s)		
	By equation (43)	By FEM	
		Lumped-mass model	Consistent-mass model
1	863·712962	863·712962	863·702760
2	863·713672	863·713672	863·704148
3	863·716748	863·716748	863·707943
4	863·725030	863·725030	863·708043
5	863·742492	863·742492	863·711542
6	863·774245	863·774245	863·724925
7	863·826534	863·826534	863·760091
8	863·906735	863·906734	863·820987
9	864·023357	864·023354	863·916315
10	864·186033	864·186026	864·055930
11	864·405519	864·405505	864·250835
12	864·693684	864·693655	864·513174

[†] Total beam length $L = 100$ m.

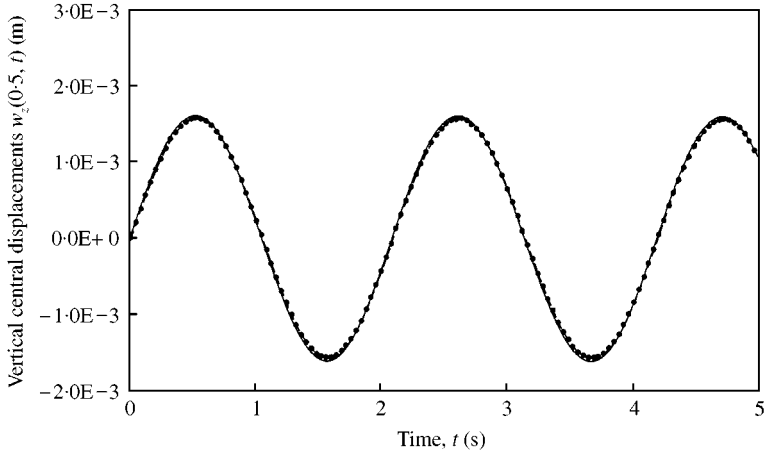

Figure 6. The time histories of a simply supported beam ($L = 100$ m) on elastic foundation subjected to a pulsating force $P(t) = \bar{P}\sin\omega_e t$ at mid-span ($\bar{P} = 98\,000$ N, $\omega_e = 3{\cdot}0$ rad/s): ——, by equation (44); – – – – –, by FEM (lumped-mass model); ●, by FEM (consistent-mass model).

5.2. NATURAL FREQUENCIES AND MODE SHAPES FOR THE RAILWAY

For the free-free railway with length $L = 500$ m (and total number of finite elements $N_e = L/\ell = 500$) studied in all the follwoing subsections, the natural frequencies and mode shapes for the 1st, 4th and 10th modes are shown in Figure 7. From the figure, one sees that $\omega_1 \approx \omega_4 \approx \omega_{10} \approx 863{\cdot}712$ rad/s, this is because the natural frequencies for a railway will approach a continuous frequency spectrum when the ratio L/γ_g of the railway exceeds a certain value (e.g., $L/\gamma_g = 500/0{\cdot}032 > 15000$ for the present example) as shown in reference [15]. Besides, Figure 7 shows that all the higher mode shapes of the railway look

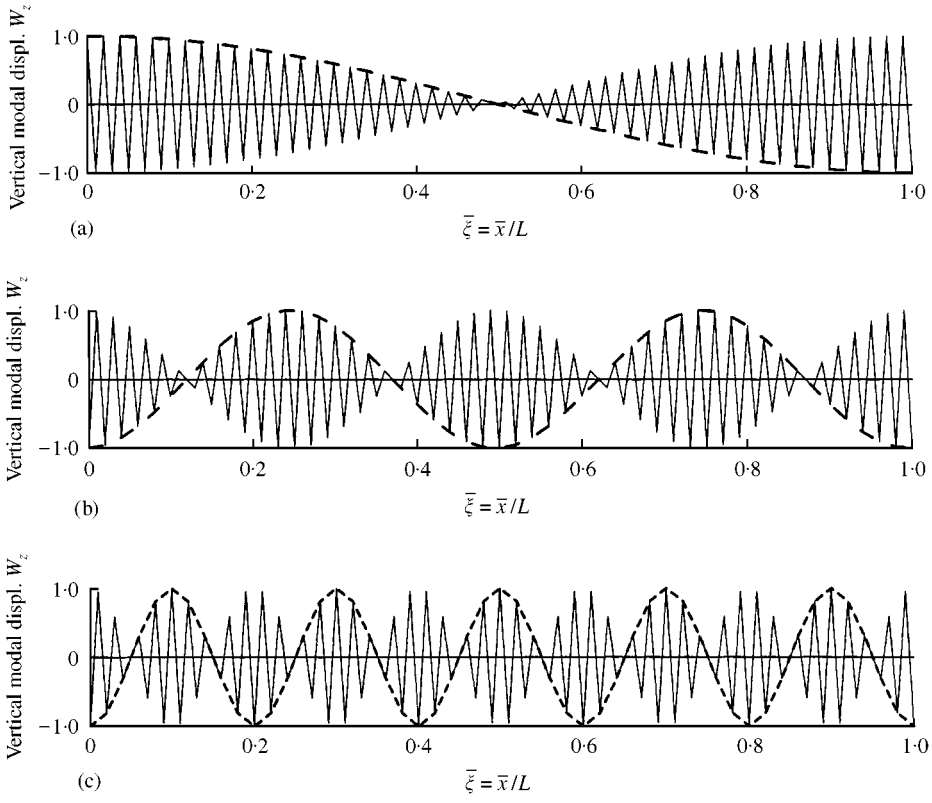

Figure 7. The mode shapes for the free–free railway with length $L = 500$ m: (a) the 1st mode with $\omega_1 = 863{\cdot}712913$ *r/s*; (b) the 4th mode with $\omega_4 = 863{\cdot}712915$ *r/s*; (c) the 10th mode with $\omega_{10} = 863{\cdot}713030$ *r/s*.

like the travelling waves with wave length

$$\lambda_k = \frac{L}{(k/2)} = \frac{2L}{k}, \quad k = 1, 2, \ldots, \tag{46}$$

where k refers to the kth mode shape. It is evident that if the resonance occurs at the kth mode, then the associated exciting period will be

$$T_{ek} = \frac{\lambda_k}{V} = \frac{2L}{kV} \tag{47}$$

or the exciting frequency is given by

$$\omega_{ek} = \frac{2\pi}{T_{ek}} = k\frac{\pi V}{L}. \tag{48}$$

Equation (48) denotes the exciting frequency "on the carriage" due to the wavy surface of the railway. Because of interaction between the railway and the carriage, the exciting frequency "on the railway" is also ω_{ek}. Equations (47) and (48) are obtained based on the assumption that the roller of the single-roller carriage always keeps "smooth" contact with the railway, hence, they are also valid for a carriage with two axle rollers. However, for the carriage with more than "two" rollers, equations (47) and (48) will be valid only for the cases

of uniformly distributed rollers with average stiffness of the suspension system near the rollers being so small that constant contact of all the rollers with the railway is not prevented. In other words, resonance of the carriage with two rollers occurs at the exciting frequency ω_{ek} defined by equation (48), but this is not always true for the carriage with more than two rollers, as one may see in the following subsections.

5.3. INFLUENCE OF TOTAL NUMBER OF AXLE ROLLERS ($\bar{n}$)

For the cases of total number of axle rollers $\bar{n} = 2$, 3 and 4, the relationship between the moving speeds of the carriage (V) and the absolute values of the maximum vertical central displacements of the railway, $|w_z(0{\cdot}5, t)|_{max}$, is shown in Figure 8(a), while the relationship between carriage speeds V and the absolute values of the maximum vertical displacements at the center of gravity (G) of carriage, $|w_G(t)|_{max}$, is shown in Figure 8(b). The time interval for the finite element analysis is $\Delta t = \ell/V$ s and the CPU time required for each curve of Figures 8–15 is about 50 h, where the unit of V is m/s and the computer machine is Digital DEC800. Some significant phenomena and the associated physical meanings are stated below:

(i) The values of $|w_z(0{\cdot}5, t)|_{max}$ decrease with the increase of $\bar{n}$ for $V < 125$ m/s (see Figure 8(a)).

For the present example, the total mass of the carriage is $m_{ev} = 2{\cdot}0 \times 10^4$ kg and the mass of each roller is $m_i = 100$ kg ($i = 1, 2, \ldots, \bar{n}$). The ratio between m_{ev} and m_i is $R_m = m_{ev}/m_i = 200{\cdot}0$. Since the mass of the carriage is much larger than that of each roller, the influence of the roller weight on the magnitude of each concentrated load on the railway $\bar{F}_{\bar{z}i}$ ($i = 1$–$\bar{n}$) defined by equation (24) is negligible, that is, $\bar{F}_{\bar{z}i} \propto m_{ev}g/\bar{n}$. From the last expression, one sees that the magnitude of each concentrated load on the railway, $\bar{F}_{\bar{z}i}$, decreases with the increase of the total number of rollers, $\bar{n}$, so do the maximum vertical central displacements of the railway, $|w_z(0{\cdot}5, t)|_{max}$.

(ii) Near $V = 50$ m/s, resonance occurs for the carriage with two rollers, but does not occur for the carriage with 3 or 4 rollers (see Figure 8(b)).

For the 10th mode shape of the present railway (see Figure 7(c)), from equations (46) and (47) one has $\lambda_{10}/2 = L/k = 500/10 = 50$ m and $T_{e10}/2 = L/(\text{kV}) = 500/(10\,\text{V}) = 50/\text{V}$ s. Hence, for a carriage with two rollers and travelling on the railway with speed $V = 50$ m/s, it will be like a two-wheel motorcycle running on a road with sinusoidal (wavy) surface and its framework (or body) will oscillate regularly in the vertical direction with half period $T_{e10}/2 = 50/\text{V} = 50/50 = 1{\cdot}0$ s. This should be the reason why the solid curve for the "two-roller" carriage as shown in Figure 8(b) has a hump (or has the resonant phenomenon) near travelling speed $V = 50$ m/s. However, for the carriage with 3 or 4 rollers, the non-uniform distribution or the particular arrangement of the rollers prevents the "smooth" contact (or "exact" fit) of "all the rollers" with the wavy profile of the 10th mode shape. Thus, the "regular" oscillation of the carriage in the vertical direction for the carriage with rollers more than "two" is significantly reduced, so that the resonance near $V = 50$ m/s does not occur.

It is noted that, for a "rigid" carriage with "two" rollers, "all the rollers" will contact with the railway freely, but this is not "always" true for a "rigid" carriage with more than two rollers. Besides, for the example studied in this paper, the magnitudes and locations of all the suspension systems are "symmetrical" with respect to the

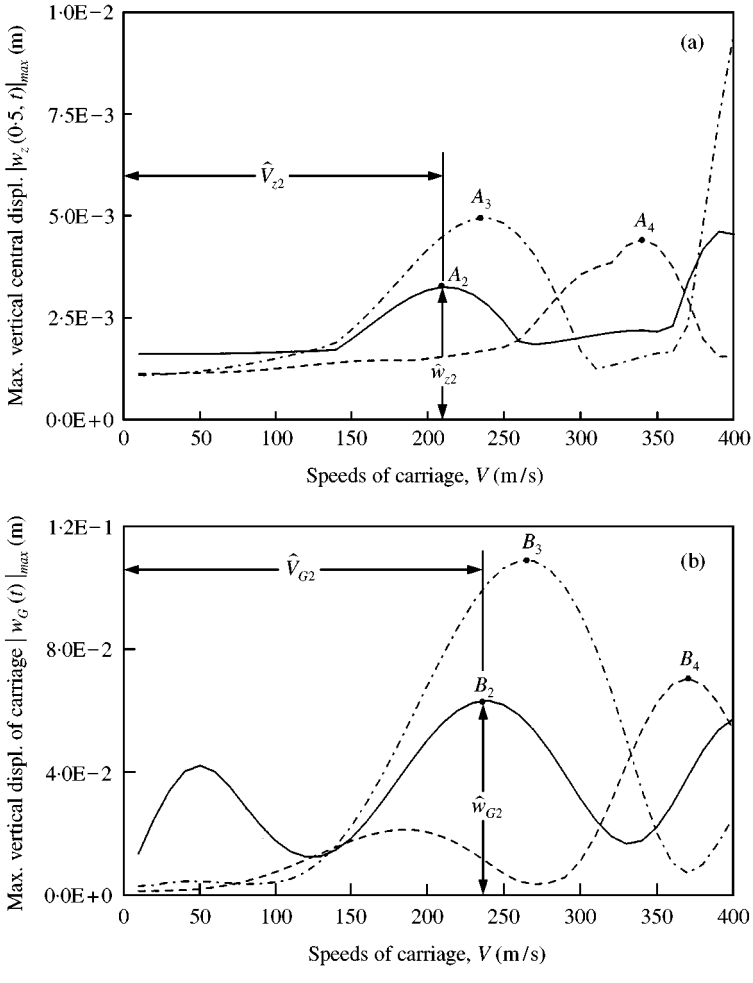

Figure 8. Effect of total number of rollers for a carriage, $\bar{n}$, on (a) the maximum vertical central displacement of the railway, $|w_z(0{\cdot}5, t)|_{max}$ and (b) the maximum vertical displacement at the c.g. (G) of the carriage, $|w_G(t)|_{max}$: ——, 2-roller carriage ($r_1 = -r_2 = 6$ m); – · – · –, 3-roller carriage ($r_1 = -r_2 = 5$ m, $r_3 = 0$ m); – – – –, 4-roller carriage ($r_1 = -r_4 = 5$ m, $r_2 = -r_3 = 4$ m).

center of gravity of the carriage, G; therefore, the heave and pitch motions of the carriage are uncoupled and the natural frequency of the heave motion and that of the pitch motion in such a case are equal to each other [23]. In general, the "symmetrical" arrangement for the carriage is the situation in practice, but the presented theory is not limited to the "symmetrical" cases. Actually, for the passengers in a "long" carriage, they usually do not feel the existence of the pitch motion of the carriage because the amplitudes of the deflected wavy railway surface induced by the moving carriage are much smaller than the carriage length.

(iii) The resonant speed for railway, $\hat{V}_{zi}$, and that for carriage, $\hat{V}_{Gi}$, increase with the increase of total roller number $\bar{n}$ (See Figures 8(a) and (b)).

In Figure 8(a), the maximum of each curve is denoted by A_i ($i = 2, 3, 4$) and in Figure 8(b) by B_i ($i = 2, 3, 4$), where i refers to the total number of rollers for each carriage, $\bar{n}$. For convenience, the value of $|w_z(0{\cdot}5, t)|_{max}$ for A_i is called "peak maximum railway displacement" and denoted by $\hat{w}_{zi}$, while the associated carriage

speed is called the "peak maximum-displacement speed for railway" (or resonant speed for railway) and denoted by $\hat{V}_{zi}$. Similarly, $\hat{w}_{Gi}$ and $\hat{V}_{Gi}$ are called "peak maximum carriage displacement" and "peak maximum-displacement speed for carriage" (or resonant speed for carriage), respectively. It is noted that the foregoing "peak maximum displacements" denote those at the specified points and do not mean that they are the "overall" (or global) maximum displacements in the whole railway or in the whole carriage.

From Figure 8(b) one sees that the resonant speed for carriage $\hat{V}_{Gi}$ increases with the increase of roller number $\bar{n}$. In other words, the larger the total number of rollers for a carriage, $\bar{n}$, the higher the resonant speed for carriage, $\hat{V}_{Gi}$. This is because the undamped heave and pitch natural frequency of the carriage is given by $\omega_c = \sqrt{\sum_{i=1}^{\bar{n}} k_i/m_{ev}}$, so that the heave and pitch natural frequency of the carriage increases with the increase of roller number $\bar{n}$; besides, the exciting frequency ω_{ek} is proportional to the carriage speed V as shown in equation (48). Since the responses of the railway are induced by the carriage, the relationship between the resonant speed for railway, $\hat{V}_{zi}$, and the total roller number $\bar{n}$ (see Figure 8(a)) is similar to that between the resonant speed for carriage, $\hat{V}_{Gi}$, and $\bar{n}$ (see Figure 8(b)).

(iv) The resonant speeds for the railway, $\hat{V}_{zi}$, are not equal to the corresponding ones for the carriage, $\hat{V}_{Gi}$ (see Figures 8(a) and 8(b)).

From Figures 8(a) and 8(b), one sees that the peak maximum railway displacements $\hat{w}_{zi}$ are much smaller than the corresponding peak maximum carriage displacements $\hat{w}_{Gi}$. This is a reasonable result, since the stiffness of the suspension system for the carriage is much smaller than the stiffness of the elastic foundation for the railway. In addition, because of the effect of the suspension system, the peak maximum railway displacements $\hat{w}_{zi}$ and the corresponding peak maximum carriage displacements $\hat{w}_{Gi}$ do not appear at the same instant of time as one may see from the histories of $w_z(0{\cdot}5, t)$ and $w_G(t)$. This is the main reason why the resonant speeds for the railway, $\hat{V}_{zi}$, are not equal to the corresponding ones for the carriage, $\hat{V}_{Gi}$, as shown in Figures 8(a) and 8(b). From the last two figures one finds that $\hat{V}_{Gi} - \hat{V}_{zi} \approx 25$ m/s for the total number of rollers $i = 2, 3$ and 4.

5.4. INFLUENCE OF ROLLER SPACING

Let r_i ($i = 1 - \bar{n}$) denote the distance between the ith roller and the c.g. of the carriage, G, as shown in Figure 3, the influence of the roller spacing $d_{ij} = r_i - r_j$ on the maximum vertical central displacements of the railway, $|w_z(0{\cdot}5, t)|_{max}$, with the total number of rollers, $\bar{n} = 2$ and $\bar{n} = 4$, are shown in Figures 9(a) and 9(b), respectively. It is noted that the value of r_i for the ith roller located on the left side of the c.g. of the carriage, G, is positive, while the value of r_i on the right side of G is negative as shown by the statement following equation (9). The maxima for the three curves of Figure 9(a) are denoted by A_2', A_2'' and A_2''', respectively, where the subscript 2 refers to the carriage with "two" rollers and the superscripts (primes) $'$, $''$ and $'''$ denote the carriage with roller spacings $d_{ij} = r_i - r_j = 12, 10$ and 8 m, respectively. From Figure 9(a) one sees that the resonant speed for railway, $\hat{V}_{zi}$, increases with reducing the roller spacing d_{ij}. From reference [15] one finds that there exists a critical speed $V_{cr} \approx 707$ m/s for the present railway subjected to a "single" moving force, which is much higher than the carriage speed shown in Figure 9. It is believed that this result may be used to explain the above trend of $\hat{V}_{zi}$, since the "two" rollers will be equivalent to a "single" roller when the spacing d_{ij} decreases and approaches zero (i.e., $d_{ij} \to 0$).

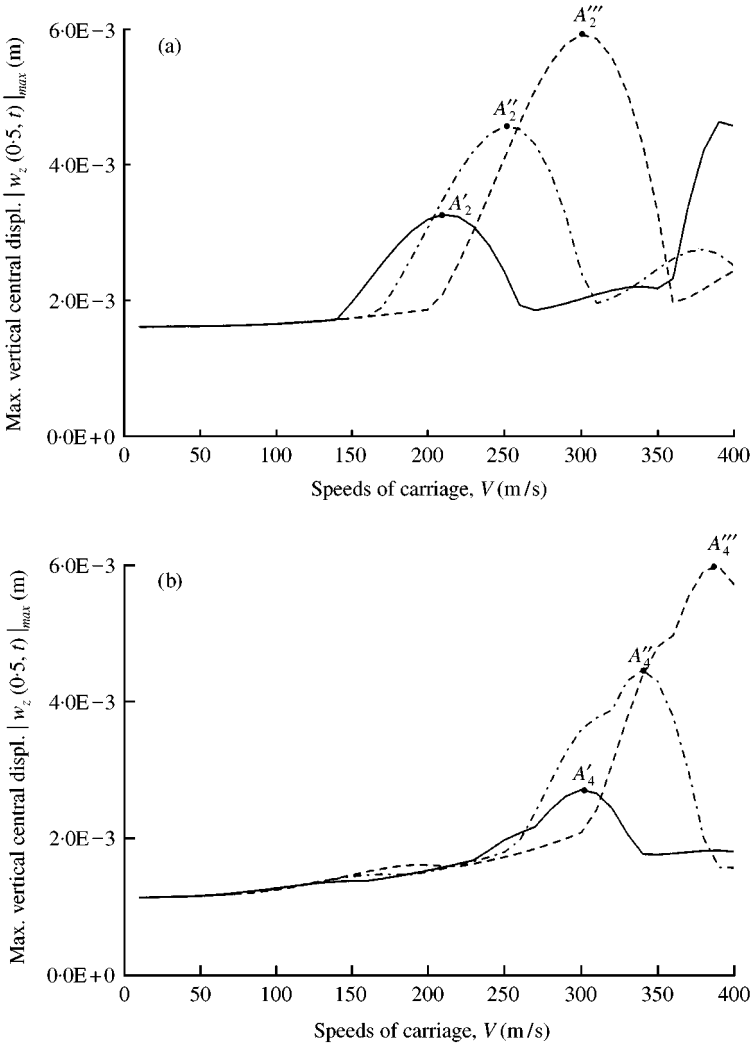

Figure 9. Influence of roller spacing $d_{ij} = r_i - r_j$ on the maximum vertical central displacement of the railway, $|w_z(0{\cdot}5, t)|_{max}$, with the total number of rollers: (a) $\bar{n} = 2$; 2-roller carriage: ——, $r_1 = -r_2 = 6$ m; –·–·–·–, $r_1 = -r_2 = 5$ m; – – – – –, $r_1 = -r_2 = 4$ m, (b) $\bar{n} = 4$; 4-roller carriage: ——, $r_1 = -r_4 = 6$ m, $r_2 = -r_3 = 5$ m; –·–·–·–, $r_1 = -r_4 = 5$ m, $r_2 = -r_3 = 4$ m; – – – – –, $r_1 = -r_4 = 4$ m, $r_2 = -r_3 = 3$ m.

The same theory may be used to explain the phenomenon appearing in Figure 9(b) with $\bar{n} = 4$, where the maxima of the three curves are denoted by A_4', A_4'' and A_4'''. Of course, the subscript 4 denotes $\bar{n} = 4$, but the superscripts (primes) $'$, $''$ and $'''$ denote three sets of roller spacings: (i) $d_{12} = 1$ m, $d_{23} = 10$ m, $d_{34} = 1$ m; (ii) $d_{12} = 1$ m, $d_{23} = 8$ m, $d_{34} = 1$ m and (iii) $d_{12} = 1$ m, $d_{23} = 6$ m, $d_{34} = 1$ m respectively. It is evident that the major difference between the three sets of roller spacings is the values of $d_{23} = r_2 - r_3 = 10, 8, 6$ m, respectively. Because the latter are smaller than the corresponding ones for the two-roller carriage as shown in Figure 9(a), $d_{12} = r_1 - r_2 = 12, 10, 8$ m, the associated resonant speed for the railway, $\hat{V}_{zi}$, as shown in Figure 9(b) are greater than the corresponding ones in Figure 9(a). For example, the value of $\hat{V}_{zi}$ is 300 m/s for A_4' (with $d_{23} = 10$ m) as shown in Figure 9(b), but the value of $\hat{V}_{zi}$ is 215 m/s for A_2' (with $d_{12} = 12$ m) in Figure 9(a). The former is greater

than the latter, because the roller spacing for the former ($d_{23} = 10$ m) is smaller than the spacing for the latter ($d_{12} = 12$ m).

The influence of roller spacing d_{ij} on the maximum vertical displacement at c.g. of the carriage, $|w_G(t)|_{max}$, is shown in Figure 10. Where the maxima for the curves with $\bar{n} = 2$ are denoted by B_2', B_2'' and B_2''' (see Figure 10(a)) and those with $\bar{n} = 4$ by B_4', B_4'' and B_4''' (see Figure 10(b)). It is evident that the resonant speed for the carriage, $\hat{V}_{Gi}$, increases with decreasing the roller spacing. This trend of the curves for $\hat{V}_{Gi}$ versus roller spacing d_{ij} (Figure 10) is the same as that for $\hat{V}_{zi}$ versus d_{ij} (Figure 9) due to the effect of interaction between the carriage and the railway.

From Figure 10(a) one also sees that the 2-roller carriage has the phenomenon of resonance in the vicinity of $V = 50$ m/s and the resonance becomes more predominant when the roller spacing d_{12} decreases from 12 to 8 m. The reason for the resonance of

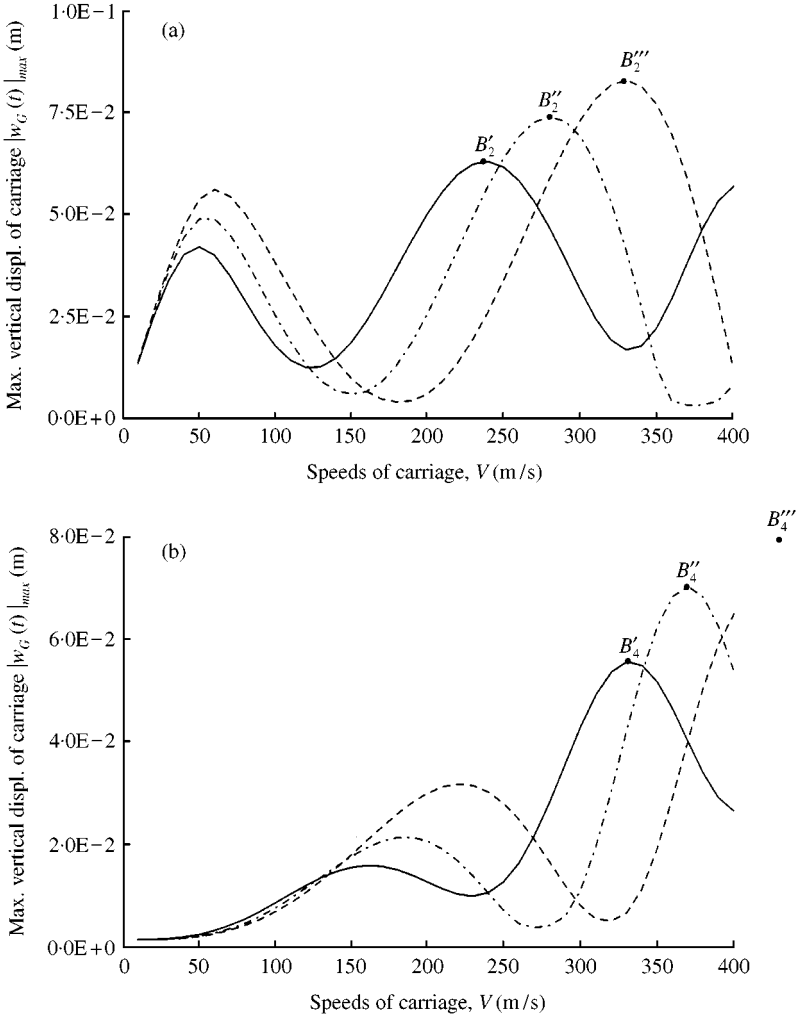

Figure 10. Influence of roller spacing $d_{ij} = r_i - r_j$ on the maximum vertical displacement at c.g. (G) of the carriage, $|w_G(t)|_{max}$, with the total number of rollers: (a) $\bar{n} = 2$; 2-roller carriage: ——, $r_1 = -r_2 = 6$ m; –·–·–·, $r_1 = -r_2 = 5$ m; – – – – –, $r_1 = -r_2 = 4$ m, (b) $\bar{n} = 4$; 4-roller carriage: ——, $r_1 = -r_4 = 6$ m, $r_2 = -r_3 = 5$ m; –·–·–·, $r_1 = -r_4 = 5$ m, $r_1 = -r_4 = 4$ m; – – – – –, $r_1 = -r_4 = 4$ m, $r_2 = -r_3 = 3$ m.

a 2-roller carriage at $V \approx 50$ m/s has been stated in the last subsection (see Figure 8(b)), and the reason for smaller spacing inducing more predominant resonance is described below. In the derivation of equations (47) and (48), it has been shown that the two expressions defining the values of exciting period T_{ek} and exciting frequency ω_{ek} are obtained from the carriage with "single" roller. Hence, for a two-roller carriage, if the spacing d_{12} approaches zero, the dynamic behavior of the two-roller carriage will approach that of the single-roller carriage. From this point of view, the influence of roller spacing d_{ij} on the values of $|w_G(t)|_{max}$ in the vicinity of $V = 50$ m/s as shown in Figure 10(a) is reasonable.

5.5. EFFECT OF STIFFNESS OF THE SUSPENSION SYSTEM

The stiffness of the suspension system is determined by the spring constant k as shown in Figures 3 and 4. For the cases of $k = 30\,000$, $60\,000$ and $90\,000$ N/m, Figure 11 shows the

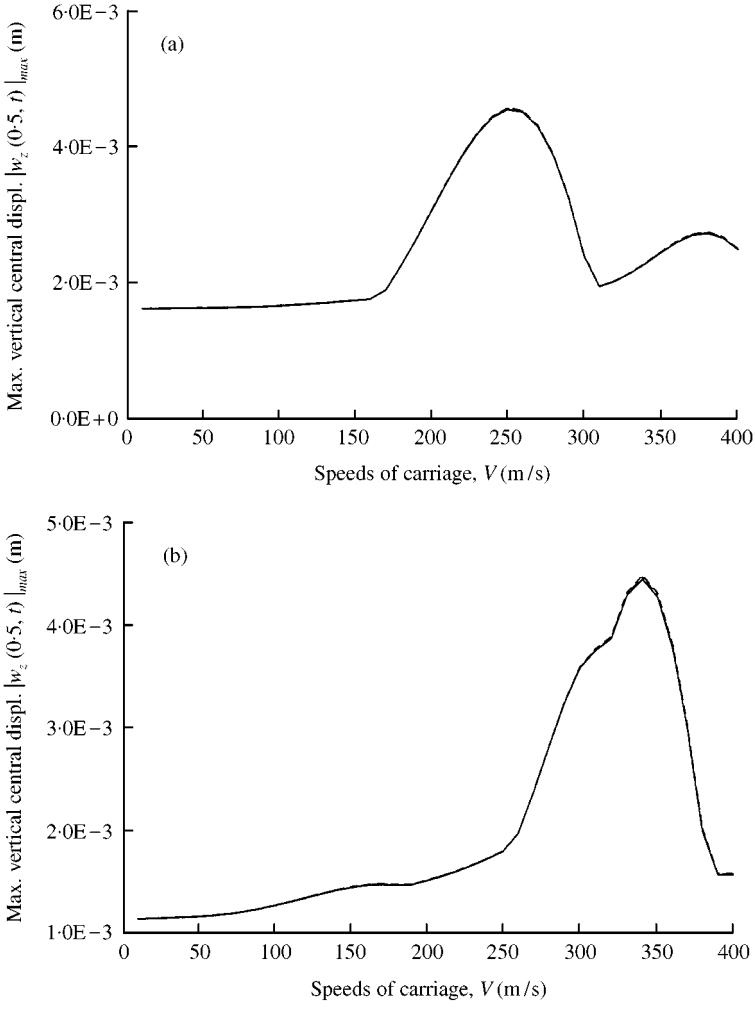

Figure 11. Effect of stiffness of the suspension system, k, on the maximum vertical central displacements of railway, $|w_z(0{\cdot}5, t)|_{max}$, due to the action of (a) 2-roller carriage with roller locations $r_1 = -r_2 = 5$ m and (b) 4-roller carriage with $r_1 = -r_4 = 5$ m and $r_2 = -r_3 = 4$ m: ——, $k = 30\,000$ N/m; –·–·–·, $k = 60\,000$ N/m; – – – – –, $k = 90\,000$ N/m.

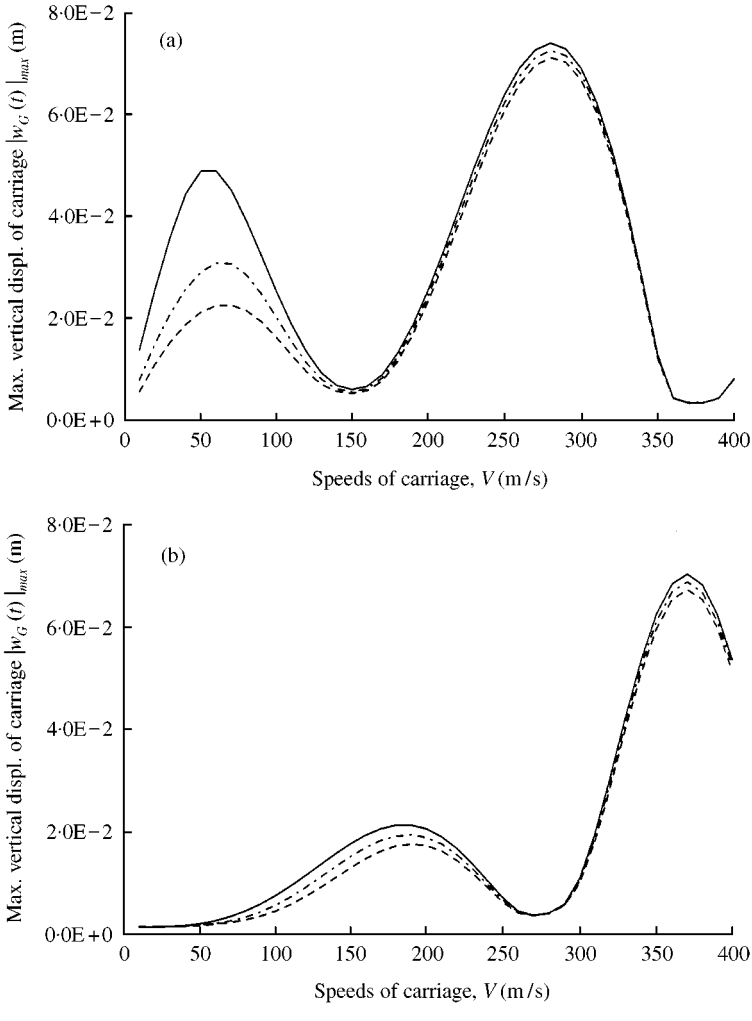

Figure 12. Effect of stiffness of the suspension system, k, on the maximum vertical displacements at c.g. of the carriage, $|w_G(t)|_{max}$, due to the action of (a) 2-roller carriage with roller locations $r_1 = -r_2 = 5$ m and (b) 4-roller carriage with $r_1 = -r_4 = 5$ m and $r_2 = -r_3 = 4$ m: ——, $k = 30\,000$ N/m; –·–·–·–, $k = 60\,000$ N/m; – – – – –, $k = 90\,000$ N/m.

curves for $|w_z(0{\cdot}5, t)|_{max}$ versus V and Figure 12 shows those for $|w_G(t)|_{max}$ versus V. Among the curves, those in Figures 11(a) and 12(a) are due to action of the 2-roller carriage with spacing $d_{12} = r_1 - r_2 = 10$ m, while those in Figures 11(b) and 12(b) are due to the 4-roller carriage with spacings $d_{12} = 1$ m, $d_{23} = 8$ m and $d_{34} = 1$ m. Since the three curves in Figure 11(a) or 11(b) are approximately coincident with each other, the influence of stiffness of the suspension system on $|w_z(0{\cdot}5, t)|_{max}$ is negligible. This is a reasonable result, because, for the present example with $k_i = \text{constant}\,(i = 1\text{–}\bar{n})$, the external loads on the railway $\bar{F}_{\bar{z}i}(t)$ are independent of the spring constants $k_i\,(i = 1\text{–}\bar{n})$ as may be seen from equation (24) and the values of $k_i\,(= 3{\cdot}0 \times 10^4$ N/m) are much smaller than those of the elastic foundation for the railway, $k_w\,(= 3{\cdot}73 \times 10^7$ N/m).

Although the influence of stiffness of the suspension system on $|w_z(0{\cdot}5, t)|_{max}$ is negligible (see Figures 11(a) and 11(b)), this is not true for $|w_G(t)|_{max}$ (see Figures 12(a) and 12(b)),

however. From Figures 12(a) and 12(b) one sees that the peak maximum carriage displacements, $\hat{w}_{Gi}$ $(i = 1–\bar{n})$, decrease with the increase of spring constants k_i $(i = 1–\bar{n})$; besides, the values of $\hat{w}_{Gi}$ $(i = 1–\bar{n})$ due to the 2-roller carriage (see Figure 12(a)) are greater than the corresponding ones due to the 4-roller carriage (see Figure 12(b)).

5.6. INFLUENCE OF CARRIAGE MASS

For the case of carriage mass much greater than the roller mass (i.e., $m_{ev} \gg m_i$, $i = 1–\bar{n}$), such as the present example, equation (24) shows that the external exciting forces on the railway, $\bar{F}_{\bar{z}i}$ $(i = 1–\bar{n})$, are approximately proportional to the magnitude of the carriage mass m_{ev}. This is the main reason why the values of the maximum vertical central displacements of the railway, $|w_z(0{\cdot}5, t)|_{max}$, as shown in Figure 13 are also proportional to the magnitude of

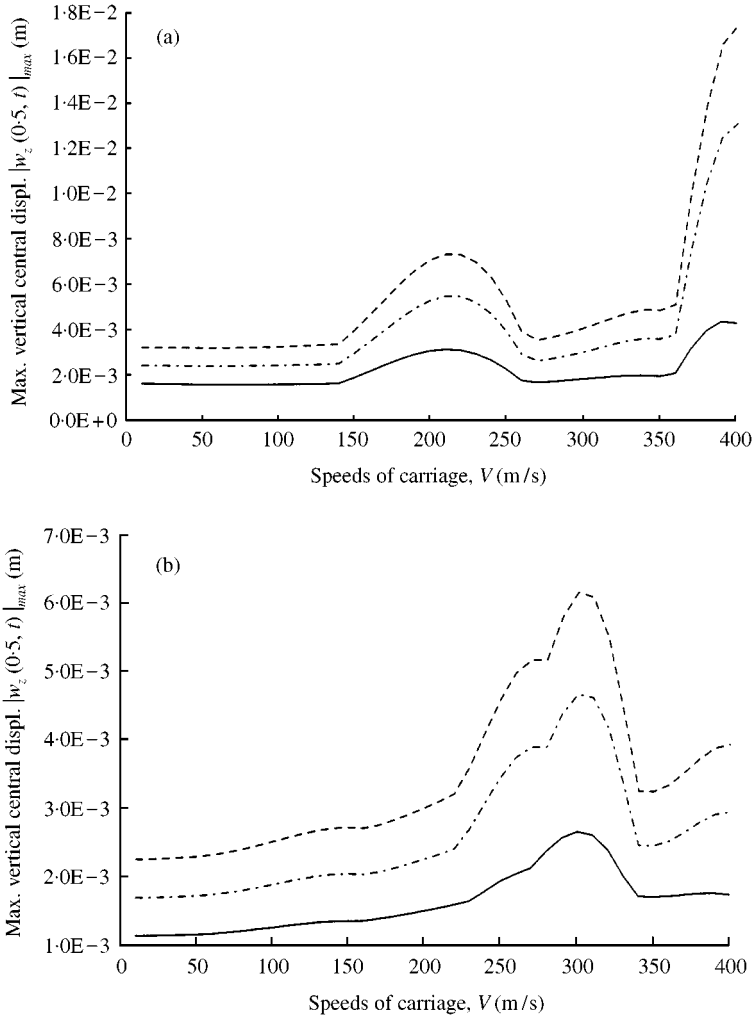

Figure 13. Influence of carriage mass m_{ev} on the maximum vertical central displacements of the railway, $|w_z(0{\cdot}5, t)|_{max}$, due to (a) 2-roller carriage with roller locations $r_1 = -r_2 = 6$ m and (b) 4-roller carriage with $r_1 = -r_4 = 6$ m and $r_2 = -r_3 = 5$ m: ——, $m_{ev} = 20\,000$ kg; –·–·–·, $m_{ev} = 30\,000$ kg; – – – – –, $m_{ev} = 40\,000$ kg.

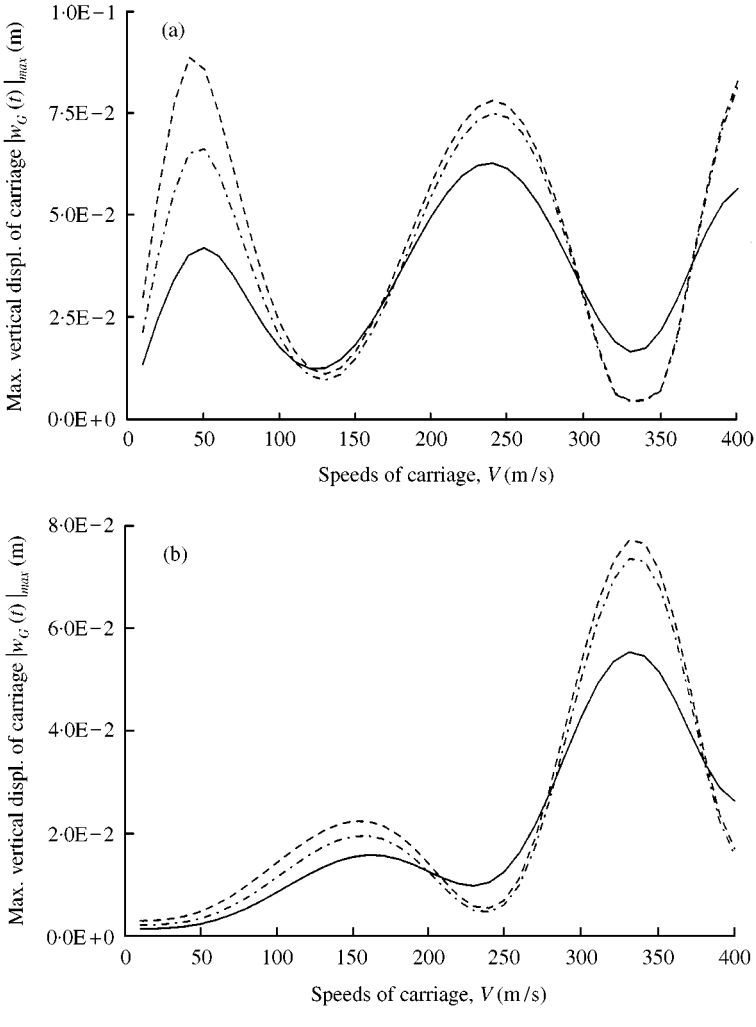

Figure 14. Influence of carriage mass m_{ev} on the maximum vertical displacements at c.g. of the carriage, $|w_G(t)|_{max}$, due to (a) 2-roller carriage with roller locations $r_1 = -r_2 = 6$ m and (b) 4-roller carriage with $r_1 = -r_4 = 6$ m and $r_2 = -r_3 = 5$ m: ——, $m_{ev} = 20\,000$ kg; –·–·–·, $m_{ev} = 30\,000$ kg; – – – – –, $m_{ev} = 40\,000$ kg.

m_{ev}, approximately, either the railway is subjected to the 2-roller carriage with $r_1 = -r_2 = 6$ m (Figure 13(a)) or the 4-roller carriage with $r_1 = -r_4 = 6$ m and $r_2 = -r_3 = 5$ m (Figure 13(b)).

A similar phenomenon appears in Figure 14(a) in the vicinity of $V = 50$ m/s and in Figure 14(b) in the vicinity of $V = 150$ m/s for the maximum vertical displacements at the c.g. of carriage, $|w_G(t)|_{max}$. But this similarity disappears in the vicinity of $V = 240$ m/s in Figure 14(a) and $V = 330$ m/s in Figure 14(b), because the values of $|w_G(t)|_{max}$ are not proportional to the carriage mass m_{ev} again, near the above-mentioned speed ranges. This should be the result of interaction between the railway and the carriage. Besides, the values of $|w_G(t)|_{max}$ decrease with the increase of carriage mass m_{ev} in the vicinity of $V = 130$ m/s in Figure 14(a) and $V = 230$ m/s in Figure 14(b), near which the minimum of each curve is located. This phenomenon means that the stability of the carriage will increase with the increase of carriage mass m_{ev} in the speed range far from resonance.

5.7. INFLUENCE OF DISTRIBUTIONS OF ROLLERS

In this subsection, the dynamic behaviors of the railway and the carriage due to the action of a 4-roller carriage with two kinds of roller distributions are studied. As shown in Figure 15, the solid curves are obtained based on the "non-uniform" distribution of the four rollers along the carriage length with locations $r_1 = -r_4 = 6\,\text{m}$, $r_2 = -r_3 = 5\,\text{m}$ (or $d_{12} = 1\,\text{m}$, $d_{23} = 10\,\text{m}$, $d_{34} = 1\,\text{m}$), while the dashed curves are based on the "uniform" distribution with locations $r_1 = -r_4 = 6\,\text{m}$, $r_2 = -r_3 = 2\,\text{m}$ (or $d_{12} = d_{23} = d_{34} = 4\,\text{m}$). For convenience, the non-uniformly distributed rollers are called "non-uniform rollers" and the carriage with non-uniform rollers is called the "non-uniform carriage". Similarly, "uniform rollers" refers to the uniformly distributed rollers and "uniform carriage" refers to the carriage with uniform rollers.

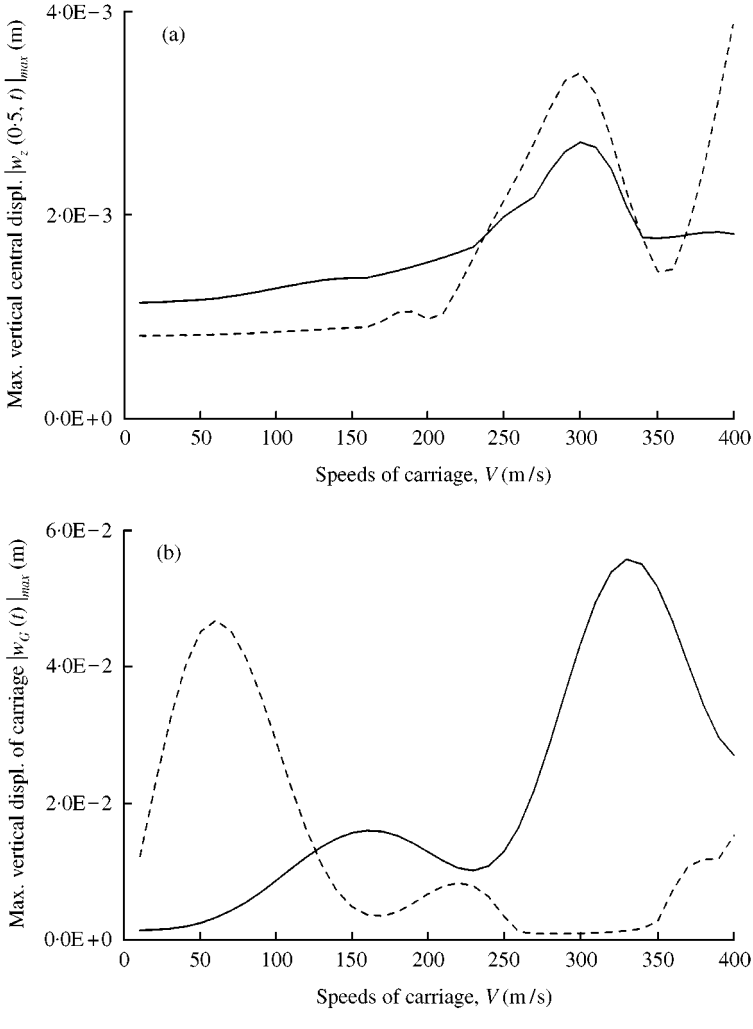

Figure 15. Influence of uniform and non-uniform distributions of rollers along the carriage length on (a) the maximum vertical central displacements of the railway, $|w_z(0 \cdot 5, t)|_{max}$, and (b) the maximum vertical displacements at c.g. of the carriage, $|w_G(t)|_{max}$. 4-roller carriage: ——, $r_1 = -r_4 = 6\,\text{m}$, $r_2 = -r_3 = 5\,\text{m}$; – – – – –, $r_1 = -r_4 = 6\,\text{m}$, $r_2 = -r_3 = 2\,\text{m}$.

For the non-uniform carriage, roller 1 is very close to roller 2 ($d_{12} = 1$ m < 2 m) and so also for roller 3 and roller 4 ($d_{34} = 1$ m < 2 m), hence the effect of interaction between rollers 1 and 2 is predominant and so also for rollers 3 and 4. However, for the uniform carriage, the spacing between any two adjacent rollers is so large ($d_{12} = d_{23} = d_{34} = 4$ m > 2 m) that the interactive effect between any two adjacent rollers is negligible [15]. This is the reason why the maximum vertical central displacements of the railway, $|w_z(0{\cdot}5, t)|_{max}$, due to the action of the "non-uniform carriage" are larger than those due to the "uniform carriage" in the speed range far from resonance, $V = 0$–235 m/s, as shown in Figure 15(a). But this is not true for the speed range near resonance, $V = 235$–335 m/s. This is because the excitations on the railway coming from the non-uniform carriage (or rollers) are irregular and those from the uniform carriage (or rollers) are regular.

From Figure 15(b) one sees that the influence of roller distribution on the maximum vertical displacements at c.g. of the carriage, $|w_G(t)|_{max}$, is opposite to that on the maximum vertical central displacement of the railway, $|w_z(0{\cdot}5, t)|_{max}$, just mentioned above (see Figure 15(a)). Whether for non-uniform carriage or uniform carriage, the distributions of the four rollers are "symmetric" with respect to the c.g. (G) of the carriage, hence the undamped heave and pitch natural frequencies of the carriages are the same [23] and given by $\omega_c = \sqrt{\sum_{i=1}^{4} k_i/m_{ev}}$. Now that resonance occurs on the "uniform carriage" and does not occur on the "non-uniform carriage" in the vicinity of $V \approx 50$ m/s, this phenomenon reveals the fact that the exciting frequency (ω_e) on the carriage coming from the railway through the uniform rollers due to the interactive effect between railway and carriage is different from that through the non-uniform rollers. In other words, the heave and pitch natural frequency of the uniform carriage is the same as that of the non-uniform carriage, but the exciting frequencies associated with the uniform rollers are different from those associated with the non-uniform rollers. This is the reason why resonance occurs on the uniform carriage and does not occur on the non-uniform carriage in the vicinity of $V \approx 50$ m/s. On the contrary, in the vicinity of $V \approx 330$ m/s, resonance occurs on the non-uniform carriage and does not occur on the uniform carriage as shown in Figure 15(b). The reason why resonance will occur on the 4-roller uniform carriage in the vicinity of $V \approx 50$ m/s is stated as follows.

For the uniform carriage, its four rollers are uniformly distributed along the carriage length. Besides, the spacing between any two adjacent rollers is so large, $d_{12} = d_{23} = d_{34} = 4$ m, that the constant contact of "all the four rollers" with the 10th (wavy) mode shape (with half wavelength $\lambda_{10}/2 = 50$ m) is not prevented and the vertical motion of the 4-roller "uniform carriage" is similar to that of the "2-roller" carriage travelling along the railway. This should be the reason why the dynamic behavior of the "4-roller" uniform carriage is similar to that of the "2-roller" carriage in the vicinity of $V \approx 50$ m/s. On the contrary , for the non-uniform carriage, the spacing between rollers 1 and 2 and that between rollers 3 and 4 are so small ($d_{12} = d_{34} = 1$ m), that the average stiffness of the suspension system per unit carriage length near rollers 1 and 2, or rollers 3 and 4, is $\bar{k} = (k_1 + k_2)/d_{12} = (k_3 + k_4)/d_{34} = 6{\cdot}0 \times 10^4$ N/m, which is two times that for the uniform carriage ($\bar{k} = k_i = 3{\cdot}0 \times 10^4$ N/m). Non-uniform roller distribution plus non-uniform (stronger) stiffness for the non-uniform carriage will prevent the "smooth" contact (or "exact" fit) of "all the four rollers" with the wavy profile of the 10th mode shape of the railway and significantly change the dynamic characteristics of the non-uniform carriage.

6. CONCLUSIONS

1. For the example studied in this paper, the magnitudes and locations of all the suspension systems are "symmetrical" with respect to the center of gravity of the carriage, G,

therefore, the heave and pitch motions of the carriage are uncoupled and the natural frequency of the heave motion and that of the pitch motion are equal to each other. In general, the "symmetrical" arrangement for the carriage is the situation in practice, but the presented theory is not limited to the "symmetrical" cases.

2. Since each higher mode shape of a long railway looks like a travelling wave and all the rollers of a 2-roller carriage keep constant contact with the "wavy" higher mode shape freely, serious vertical vibration (or resonance) of the 2-roller carriage will occur if the carriage travels on the railway with speed V such that $\lambda/V = 2{\cdot}0\,\mathrm{s}$ (or $(\lambda/2)/V = 1{\cdot}0\,\mathrm{s}$), where $\lambda/2$ is the half wavelength (or distance between any two adjacent nodes) for the mode shape of the railway. However, the last statement is usually not valid for the carriage with more than "two" rollers, which is dependent upon the distribution of the rollers along the carriage length and the magnitude of spacings between any two adjacent rollers.
3. The peak maximum-displacement speed for the railway (or resonant speed for the railway), $\hat{V}_{zi}$ and that for the carriage, $\hat{V}_{Gi}$, are different. It is found that $\hat{V}_{Gi} - \hat{V}_{zi} \approx 25\,\mathrm{m/s}$ $(i = 1\text{–}\bar{n})$ for certain cases studied in this paper, where $\bar{n}$ denotes the total number of rollers for the carriage.
4. Since the value of $\hat{V}_{zi}$ (or $\hat{V}_{Gi}$) due to the action of a single-roller carriage is much higher than that due to a multi-roller carriage, reducing the roller spacing of the multi-roller carriage will raise the resonant speed $\hat{V}_{zi}$ (or $\hat{V}_{Gi}$) of the multi-roller carriage. This is due to the fact that a multi-roller carriage will look like a single-roller carriage if the spacings between any two adjacent rollers are reduced to zero.
5. The influence of the stiffness of the suspension systems, k_i $(i = 1\text{–}\bar{n})$, on the maximum vertical central displacements of railway, $|w_z(0{\cdot}5, t)|_{max}$, is negligible, but that on the maximum vertical displacements at the c.g. of the carriage, $|w_G(t)|_{max}$, is significant near the resonant speeds.
6. Increasing the carriage mass (m_{ev}) will induce higher values of $|w_z(0{\cdot}5, t)|_{max}$, but may reduce the values of $|w_G(t)|_{max}$ near the resonant speeds. Hence, increasing the carriage mass (m_{ev}) is beneficial for achieving better stability of the carriage.
7. For a multi-roller carriage, the distribution of the rollers along the carriage length is an important factor affecting the interaction between the railway and the carriage.
8. All the statements presented in this paper are based on the numerical example studied in this paper. It is possible that part of them may not be suitable for all the other examples and this needs a further study.

ACKNOWELDGMENTS

The authors wish to acknowledge the financial support of the National Science Council, Republic of China, under the Contract Number NSC87-2622-E006-019. The kind advice of Professor J. Q. Tarn is also appreciated very much.

REFERENCES

1. E. WINKLER 1867 *Die Lehre von der Elastizitat und Fastigkeit*. Prag: Verlag H. Dominikus.
2. H. E. CRINER and G. D. MCCANN 1953 *Journal of Applied Mechanics, Transactions of the ASME* **20**, 13–22. Rails on elastic foundation under the influence of high-speed travelling loads.
3. J. T. KENNEY and PASADENA Jr 1954 *Journal of Applied Mechanics, Transactions of the ASME* **21**, 359–364. Steady-state vibrations of beam on elastic foundation for moving load.

4. A. L. FLORENCE 1965 *Journal of Applied Mechanics, Transactions of the ASME* **32**, 351–358. Traveling force on a Timoshenko beam.
5. S. P. PATIL 1988 *Journal of Engineering Mechanics* **114**(4), 688–703. Response of infinite railway track to vibrating mass.
6. D. G. DUFFY 1990 *Journal of Applied Mechanics, Transactions of the ASME* **57**, 66–73. The response of an infinite railroad track to a moving vibrating mass.
7. S. P. PATIL 1987 *International Journal of Solids Structures* **23**(12), 1615–1623. Natural frequencies of an infinite beam on a simple inertial foundation model.
8. Y. WEITSMAN 1970 *Journal of Applied Mechanics, Transactions of the ASME* **37**, 1019–1030. On foundations that react in compression only.
9. Y. WEITSMAN 1972 *International Journal of Engineering Science* **10**, 73–81. A tensionless contact between a beam and an elastic half-space.
10. G. G. ADAMS and D. B. BOGY 1975 *Journal of Applied Mechanics, Transactions of the ASME* **42**, 800–804. Steady solutions for moving loads on elastic beams with one-sided constrains.
11. J. CHOROS and G. G. ADAMS 1979 *Journal of Applied Mechanics, Transactions of the ASME* **46**, 175–180. A steadily moving load on an elastic beam resting on a tensionless Winkler foundation.
12. J. HINO, T. YOSHIMURA, K. KONISHI and N. ANANTHANARAYANA 1984 *Journal of Sound and Vibration* **96**(1), 45–53. A finite element method prediction of the vibration of a bridge subjected to a moving vehicle load.
13. J. HINO, T. YOSHIMURA and N. ANANTHANARAYANA 1985 *Journal of Sound and Vibration* **100**(4), 477–491. Vibration analysis of nonlinear beams subjected to a moving load using the finite element method.
14. J. S. WU, M. L. LEE and T. S. LAI 1987 *International Journal of Numerical Methods in Engineering* **24**, 743–762. The dynamic analysis of a flat plate under a moving load by the finite element method.
15. J. S. WU and P. Y. SHIH 1999 *Technique report, Department of Naval Architecture and Marine Engineering, National Cheng-Kung University, Tainan, Taiwan* 701, R.O.C. The dynamic behavior of a finite railway under the high-speed multiple moving forces.
16. G. MICHALTSOS, D. SOPHIANOPOULOS and A. N. KOUNADIS 1996 *Journal of Sound and Vibration* **191**(3), 357–362. The effect of a moving mass and other parameters on the dynamic response of a simply supported beam.
17. E. ESMAILZADEH and M. GHORASHI 1995 *Journal of Sound and Vibration* **184**(1), 9–17. Vibration analysis of beams traversed by uniform partially distributed moving masses.
18. D. THAMBIRATNAM and Y. ZHUGE 1996 *Journal of Sound and Vibration* **198**(2), 149–169. Dynamic analysis of beams on an elastic foundation subjected to moving loads.
19. V. V. KRYLOV 1996 *Journal of Acoustic Society of America* **100**(5), 3121–3133. Vibrational impact of high-speed trains. I. Effect of track dynamics.
20. J. S. PRZEMIENIECKI 1968 *Theory of Matrix Structural Analysis*. New York: McGraw-Hill.
21. J. S. WU and K. Z. CHEN 1995 *Journal of Sound and Vibration* **188**(3), 337–345. Dynamic analysis of a channel beam due to a moving load.
22. S. P. TIMOSHENKO, D. H. YOUNG and W. WEAVER Jr 1974 *Vibration Problems in Engineering*. New York: John Wiley & Sons, Inc.
23. J. S. WU and J. J. SHEU 1996 *Journal of Sound and Vibration* **192**(2), 495–520. An exact solution for a simplified model of the heave and pitch motions of a ship hull due to a moving load and a comparison with some experimental results.